Inorganic Chemistry
Article

Inorg. Chem. **2010**, *49*, 8709–8712 **8709**
DOI: 10.1021/ic100499d

Square Coordinated MnO_2-Units in $BiMn_7O_{12}$

Hiroshi Okamoto,[†] Naoki Imamura,[‡] Maarit Karppinen,[‡,§] Hisao Yamauchi,[‡,§] and Helmer Fjellvåg*[,†]

[†]*Centre for Materials Science and Nanotechnology, Department of Chemistry,University of Oslo, P.O.Box 1033 Blindern, NO-0315 Oslo, Norway,* [‡]*Materials and Structures Laboratory, Tokyo Institute of Technology, Yokohama 226-8503, Japan, and* [§]*Laboratory of Inorganic Chemistry, Department of Chemistry, Helsinki University of Technology,FI-02015 TKK, Finland*

Received March 16, 2010

Room temperature high-resolution synchrotron X-ray diffraction (HRSXRD) measurements were carried out on polycrystalline samples of $BiMn_7O_{12}$ and $LaMn_7O_{12}$. Rietveld refinements of HRSXRD data describe the crystal structures of both compounds in the monoclinic space group $I2/m$. The maximum entropy method-based pattern fitting (MPF) method inversion of HRSXRD data was utilized to obtain the spatial electron density (ED) distribution. Obtained results show clear differences in ED distributions around Mn−O bonds between isomorphic $BiMn_7O_{12}$ and $LaMn_7O_{12}$. The scheme of ED distributions in $BiMn_7O_{12}$ indicates the presence of orbital ordering in the MnO_2 planar arrangement that appears as prominent features in very distorted MnO_{12} and MnO_6 polyhedrons in the perovskite related structure of $[BiMn_3]_{A\text{-site}}[Mn_4]_{B\text{-site}}O_{12}$.

Introduction

In perovskite-related transition metal oxides, the d-electrons play a crucial role with respect to emerging physical properties. The spatial distribution of metal−oxygen bonds and bond strengths, that is, the coordination polyhedra (planar, tetrahedral, octahedral, etc.) and their distortions, shows a large variation throughout different oxide systems, originating from electron correlations and involving spin, charge, orbital, and lattice degrees of freedom. An objective for extensive experimental and theoretical studies is indeed to understand the electronic and resulting physical properties on the basis of atomic descriptions of key structural elements. The 1:3 *A*-site ordered $AA'_3B_4O_{12}$ takes a $2 \times 2 \times 2$ multiple unit-cell relative to the simple perovskite structure, ABO_3. Recently, investigations of $AA'_3B_4O_{12}$ have been highlighted since this structure has the very unusual feature of incorporating transition metals like Mn^{3+} and/or Cu^{2+} at the A'-site. This results in unique interactions between the A'- and *B*-site 3d metals via O 2p orbitals, see, for example, $LaMn_7O_{12}$ by Prodi et al.,[1] $LaCu_3Fe_4O_{12}$ by Long et al.,[2] $CaCu_3B_4O_{12}$ (*B* = Ti, Ge, and Sn) by Mizumaki et al.,[3] $LaMn_3B_4O_{12}$ (*B* = Cr and Ti) by Long et al.,[4] and $YMn_3Al_4O_{12}$ by Tohyama et al.[5] Furthermore, the possibility of multiferroic behavior in $BiMn_7O_{12}$ similar to that of $BiMnO_3$ has been discussed.[6−8] For $LaMn_7O_{12}$, a structural transition from monoclinic $I2/m$ to cubic $Im\bar{3}$ occurs around 380 °C, corresponding to the relaxation of a Jahn−Teller distortion for the MnO_6 octahedra.[9] $BiMn_7O_{12}$ appears in two polymorphic structures at room temperature; monoclinic $I2/m$ and cubic $Im\bar{3}$.[7,10] Our results from high-resolution synchrotron X-ray diffraction (HRSXRD) data for $BiMn_7O_{12}$ show larger displacement parameters in the Rietveld analysis than for isomorphic $LaMn_7O_{12}$. Interestingly, the abnormal behavior with large displacement parameters was found primarily for O and Mn atoms, and not for Bi in $BiMn_7O_{12}$.[10] In the current work, this abnormal behavior of $BiMn_7O_{12}$ is considered in more detail on the basis of HRSXRD data and in comparison with isomorphic $LaMn_7O_{12}$.

Experimental Section

Polycrystalline samples of $BiMn_7O_{12}$[6] and $LaMn_7O_{12}$[9] were prepared by high-pressure synthesis. Powder HRSXRD

*To whom correspondence should be addressed. E-mail: helmer.fjellvag@kjemi.uio.no.

(1) Prodi, A.; Gilioli, E.; Cabassi, R.; Bolzoni, F.; Licci, F.; Huang, Q.; Lynn, J. W.; Affronte, M.; Gauzzi, A.; Marezio, M. *Phys. Rev. B.* **2009**, *79*, 085105.
(2) Long, Y. W.; Hayashi, N.; Saito, T.; Azuma, M.; Murakani, S.; Shimakawa, Y. *Nature* **2009**, *458*, 60.
(3) Mizumaki, M.; Saito, T.; Shiraki, H.; Shimakawa., Y. *Inorg. Chem.* **2009**, *48*, 3499.
(4) Long, Y.; Saito, T.; Mizumaki, M.; Agui, A.; Shimakawa, Y. *J. Am. Chem. Soc.* **2009**, *131*, 16244.
(5) Tohyama, T.; Saito, T.; Mizumaki, M.; Agui, A.; Shimakawa, Y. *Inorg. Chem.* **2010**, *49*, 2492.
(6) Imamura, N.; Karppinen, M.; Motohashi, T.; Fu, D.; Itoh, M.; Yamauchi, H. *J. Am. Chem. Soc.* **2008**, *130*, 14948.
(7) Imamura, N.; Karppinen, M.; Yamauchi, H. *Chem. Mater.* **2009**, *21*, 2179.
(8) Mezzadri, F.; Calestan, G.; Calicchio, M.; Gilioli, E.; Bolzoni, F.; Cabassi, R.; Marezio, M.; Migliori, M. *Phys. Rev. B.* **2009**, *79*, 100106.
(9) Okamoto, H.; Karppinen, M.; Yamauchi, H.; Fjellvåg, H. *J. Solid State Sci.* **2009**, *11*, 1211.
(10) Okamoto, H.; Imamura, N.; Karppinen, M.; Yamauchi, H.; Fjellvåg, H. *J. Solid State Chem.* **2010**, *183*, 185.

Published on Web 08/27/2010

Table 1. Atomic Coordinates (x, y, z) and Isotropic Displacement Parameters B for $BiMn_7O_{12}$ (Left Panel) and $LaMn_7O_{12}$ (Right Panel) at Room Temperature[a]

atoms	sites	x, y, z	B (Å^2)	atoms	sites	x, y, z	B (Å^2)
Bi	2*a*	0, 0, 0	0.701(9)	La	2*a*	0, 0, 0	0.08(2)
Mn1	2*b*	0, 1/2, 0	1.38(5)	Mn1	2*b*	0, 1/2, 0	0.31(2)
Mn2	2*c*	0, 0, 1/2	2.21(9)	Mn2	2*c*	0, 0, 1/2	0.46(3)
Mn3	2*d*	0, 1/2, 1/2	1.62(9)	Mn3	2*d*	0, 1/2, 1/2	0.28(3)
Mn4	4*e*	1/4, 1/4, 3/4	1.91(4)	Mn4	4*e*	1/4, 1/4, 3/4	0.15(2)
Mn5	4*f*	1/4, 1/4, 1,4	0.76(3)	Mn5	4*f*	1/4, 1/4, 1,4	0.14(2)
O1	4*i*	0.3050(9), 0, 0.1617(9)	3.1(2)	O1	4*i*	0.3065(4), 0, 0.1690(4)	0.05(2)
O2	4*i*	0.3186(9), 0, −0.1749(9)	2.9(2)	O2	4*i*	0.3155(5), 0, −0.1777(5)	0.05(2)
O3	8*j*	−0.0157(9), 0.1838(9), 0.3191(9)	4.3(2)	O3	8*j*	−0.0142(3), 0.1760(3), 0.3129(3)	0.27(6)
O4	8*j*	0.1778(9), 0.3132(9), 0.0181(9)	2.2(2)	O4	8*j*	0.1735(3), 0.3095(3), 0.0155(3)	0.06(2)

[a] Space group $I2/m$. Calculated standard deviations in parentheses. $BiMn_7O_{12}$: a = 7.5199(1) Å, b = 7.3661(1) Å, c = 7.5293(1) Å, and β = 91.225(1)°. $LaMn_7O_{12}$: a = 7.5167(1) Å, b = 7.3792(1) Å, c = 7.5245(1) Å, and β = 91.283(1)°.

data at room temperature were collected with the high-resolution diffractometer at the Swiss Norwegian Beamline, BM01B, European Synchrotron Radiation Facility (ESRF) with wavelengths λ = 0.52019 Å and 0.49999 Å for $BiMn_7O_{12}$ and $LaMn_7O_{12}$, respectively. Intensity data covered the ranges $5.0° \le 2\theta \le 40.0°$ [corresponding to 0.083781 Å^{-1} $\le \sin\theta/\lambda \le$ 0.621780 Å^{-1}], and $5.0° \le 2\theta \le 35.0°$ [0.087157 Å^{-1} $\le \sin\theta/\lambda \le$ 0.57359 Å^{-1}] for $BiMn_7O_{12}$ and $LaMn_7O_{12}$, respectively. The HRSXRD data were analyzed through combination of Rietveld[11] and method-based pattern fitting (MPF)[12] methods by using the program codes RIETAN-FP[13] and PRIMA.[14] The pseudo-Voigt function formulated by Thompson et al.[15] was used in the Rietveld refinements, and MPF analysis was carried out by using 124 × 124 × 124 pixels for the structure factors, derived by the Rietveld analysis. The crystal structure and the electron density (ED) were visualized by using the program VESTA.[16] The main focus is attributed to $BiMn_7O_{12}$ for which the diffraction data fully covers the high angle region.

Results and Discussion

Figures 1a and b show the fitted HRSXRD patterns at room temperature for $BiMn_7O_{12}$ and $LaMn_7O_{12}$, respectively. The best fit was obtained for space group $I2/m$. The refined atomic coordinates are listed in Table 1. The derived figure of merits, R_{wp}, were 15.13% and 9.16%, respectively, and reliability factors based on integrated intensities, R_I were 4.98% and 2.38%. The larger R-values for $BiMn_7O_{12}$ using same structural model, may at first sight suggest a symmetry reduction for $BiMn_7O_{12}$, for example, because of off-centering of Bi ions and/or local distortions of Mn−O polyhedra induced by hybridized $6s^2$ lone-pair electrons of Bi^{3+}. However, since the largest displacement parameter is found for O atoms, see Table 1, we anticipate that the discrepancies for $BiMn_7O_{12}$ are not caused by the Bi atoms. To reveal the hidden uniqueness of $BiMn_7O_{12}$, an MPF analysis based on the observed structure factors derived from the Rietveld analysis was performed. In the MPF analysis, the crystal structures are not expressed by parameters such as fractional coordinates and atomic displacement parameters, but by the ED in the unit cell. Therefore, MPF enables us to represent features mirrored by the observed data such as

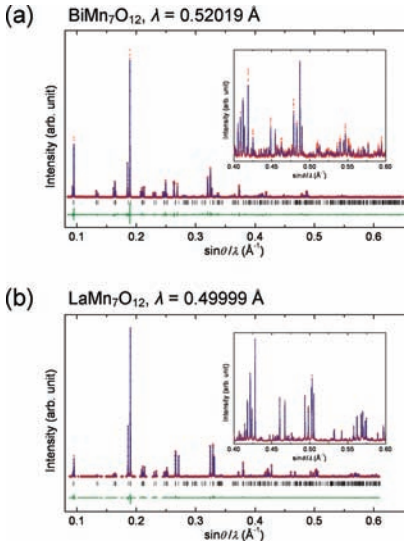

Figure 1. Rietveld profile fitting of high resolution synchrotron radiation data for (a) $BiMn_7O_{12}$ and (b) $LaMn_7O_{12}$ at room temperature, monoclinic space group $I2/m$. Insets show high angle region.

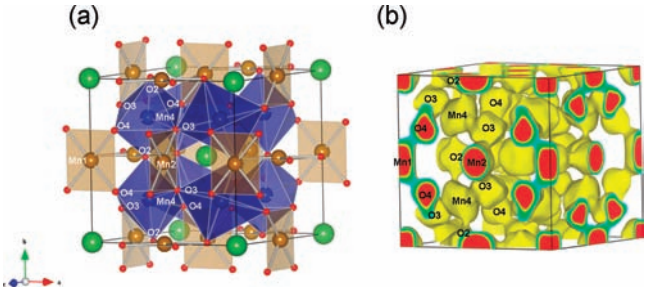

Figure 2. (a) Schematic representation of the crystal structure of (Bi/La)Mn_7O_{12}. (b) 3D equi-contour of 1 Å^{-3} density map of the ED of $BiMn_7O_{12}$.

chemical bonding, non-localized electrons, and so forth. The R_I-factors were significantly lowered after two times MPF cycling and became 3.24% and 1.83%, respectively, for $BiMn_7O_{12}$ and $LaMn_7O_{12}$.

Figures 2a and b show schematically the crystal structure of (Bi/La)Mn_7O_{12} and a corresponding 3D visualization of the calculated ED images for $BiMn_7O_{12}$, based on MPF analysis. As shown in Figure 2, the ED distribution suggests highly anisotropic bonding between the Mn and O atoms. For example, for the deformed $Mn4O_6$ octahedron, the ED shows four hybridized bonds between Mn4−O2 and

(11) Rietveld, H. *J. Appl. Crystallogr.* **1965**, *2*, 65.
(12) Izumi, F. *Solid State Ionics* **2004**, *172*, 1.
(13) Izumi, F; Momma, K. *Solid. State Phenom.* **2007**, *130*, 15.
(14) Izumi, F.; Dilanian, R. A. *Recent Research Developments in Physics*; Transworld Research Network: Trivandrum, Kerala, India, 2002; Vol. *3*, Part II, pp 699−726.
(15) Thompson, P.; Cox, D. E.; Hastings, J. B. *J. Appl. Crystallogr.* **1987**, *20*, 79.
(16) Momma, K.; Izumi, F. *J. Appl. Crystallogr.* **2008**, *41*, 653.

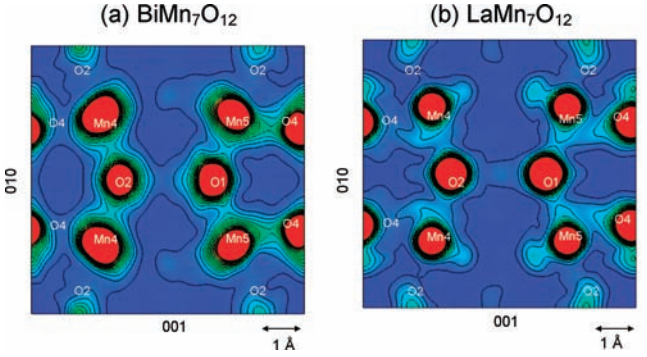

Figure 3. (0.2, 0, 0) section of 3D equi-contour of 1 $Å^{-3}$ density map of the ED of (a) $BiMn_7O_{12}$ and (b) $LaMn_7O_{12}$, respectively, with contour lines of 0 to 4 $Å^{-3}$ with 0.25 $Å^{-3}$ intervals.

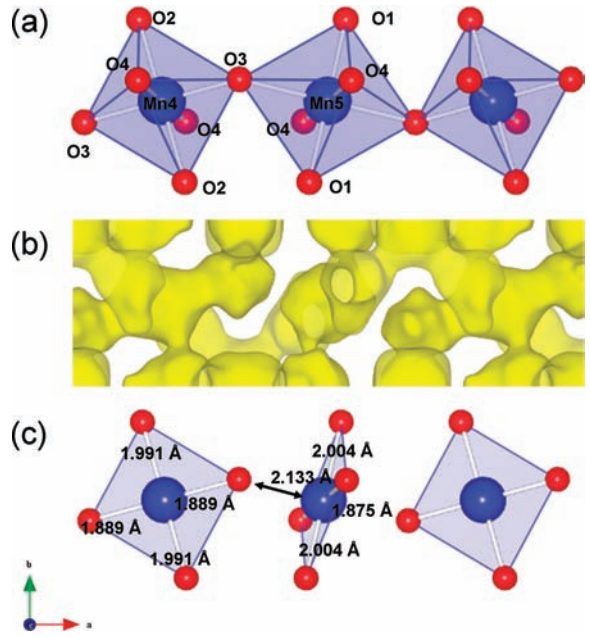

Figure 4. *B*-site MnO_6 connectivity for $BiMn_7O_{12}$ along *a*-axis; (a) schematic MnO_6 octahedra, (b) 3D equi-contour of 1 $Å^{-3}$ density map of the ED of $BiMn_7O_{12}$, and (c) representation of $d_{x^2-y^2}$-type orbital ordering within planes; longest Mn−O bonds not shown (Mn4−O4 = 2.153 Å and Mn5−O3 = 2.133 Å).

Mn4−O3, whereas no additional electron density prevails between Mn4−O4. The emphasized (0.2, 0, 0) section of the two-dimensional (2D) distribution is shown in Figures 3a and b for $BiMn_7O_{12}$ and $LaMn_7O_{12}$, respectively. For $BiMn_7O_{12}$, stronger hybridized bonds are present between Mn4−O2, whereas no such bonding features are seen between Mn4−O4. Since the MnO_6 octahedra are tilted for the *I*2/*m* symmetry these three-dimensional (3D) bonding features can not be easily identified by visual inspection of 2D cross section images such as Figures 3a and b.

Careful inspection of the 3D-like ED image of the connected MnO_6 octahedra in Figure 4 clearly reveals ED characteristic of hybridized bonding in the square coordinated $Mn4O_2$ and $Mn5O_2$ entities [i.e., between Mn4−O2 and Mn4−O3 atoms; and between Mn5−O1 and Mn5−O4 atoms]. No such features are, however, evident between the Mn4−O4 and between Mn5−O3 atoms.

Calculated geometric information of $Mn4O_6$ and $Mn5O_6$ octahedra for $BiMn_7O_{12}$ and $LaMn_7O_{12}$ is listed in Table 2.

Table 2. Geometric Information of $Mn4O_6$ and $Mn5O_6$ Octahedra; Octahedral Volume, Distortion Index, and Quadratic Elongation Index for $BiMn_7O_{12}$ and $LaMn_7O_{12}$

	$BiMn_7O_{12}$		$LaMn_7O_{12}$	
	Mn-site			
	Mn4	Mn5	Mn4	Mn5
MnO_6 volume, *v* ($Å^3$)	10.75	10.65	10.75	10.68
distortion index, D^a	0.04699	0.04275	0.04299	0.04033
quadratic elongation index, Λ^b	1.009	1.008	1.005	1.005

[a] A distortion index *D*, based on bond lengths; $D = (1/6)\sum_{i=1}^{6}|l_i - l_{average}|/|l_{average}|$. [b] Quadratic elongation index Λ, based on bond lengths; $\Lambda = (1/6)\sum_{i=1}^{6}(l_i/l_o)^2$, where l_o is the center-to-vertex distance of a regular octahedron of the same volume, calculated by VESTA.

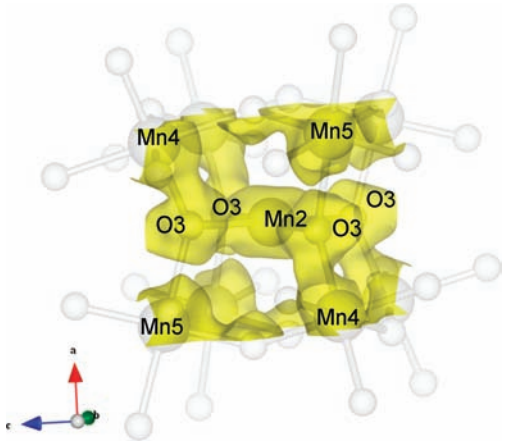

Figure 5. Local $Mn_{B\text{-site}}O_6$ and $Mn_{A\text{-site}}O_2$ connectivity for $BiMn_7O_{12}$. 3D equi-contour of 1 $Å^{-3}$ density map of the ED is shown together with schematic Mn−O bonds.

The distortion index *D*[17] indicates that Jahn−Teller distortion appears in MnO_6 for both phases. Interestingly, the MnO_6 octahedra in $BiMn_7O_{12}$ show a larger degree of distortion than $LaMn_7O_{12}$ in terms of *D* as well as in the quadratic elongation index Λ.[18] It is worth noting that the MnO_6 volume, *v*, is identical for $BiMn_7O_{12}$ and $LaMn_7O_{12}$. This is also observed for the unit-cell parameters. The calculated bond distances for the $Mn4O_6$ and $Mn5O_6$ octahedra [see Figure 4c; the longest bonds, that is, Mn4−O4 and Mn5−O3 not shown] suggest that these hybridized bonds reflect directly the four shorter bonds of the deformed octahedron, consistent with a $d_{x^2-y^2}$-type of orbital ordering of trivalent Mn ions in MnO_2 planes of the MnO_6 octahedra. Because of *I*2/*m* symmetry, the scheme of the $d_{x^2-y^2}$-type of orbital ordering in the MnO_2 plans is not parallel to the crystallographic axes. There are significant differences in the ED between $BiMn_7O_{12}$ and $LaMn_7O_{12}$ in terms of the Mn−O bonds in MnO_6 octahedra, see Figures 3a and b.

Furthermore, since trivalent Mn ions also occupy the *A*-site in $BiMn_7O_{12}$, the anisotropy with respect to chemical bonding within the *B*-site octahedra affects also the connectivity and interactions between *A*- and *B*-site Mn atoms via their common O atoms. For instance, Figure 5 shows the calculated ED distribution around the Mn2 site. There is strong hybridization governing (*i*) square coordinated MnO_2 entities between Mn2−O3 atoms and (*ii*) the Mn2−O3−Mn4 linkages,

(17) Baur, W. H. *Acta Crystallogr.* **1974**, *B30*, 1195.
(18) Robinson, K; Gibbs, G. V.; Ribbe, P. H. *Science* **1971**, *172*, 567.

whereas no such localized electron densities for observed for the Mn2−O3−Mn5 connection. This results in complex interactions between the *A*- and *B*-site Mn atoms.

Conclusions

In conclusion, we have investigated the ED distribution of $BiMn_7O_{12}$ and $LaMn_7O_{12}$ on the basis of precise crystal structure analysis of high resolution synchrotron radiation diffraction data. Dominant in-plane covalent bonding for *A*-site MnO_4 and *B*-site distorted MnO_6 is evident for $BiMn_7O_{12}$. A clear difference in the degree of such covalent bonding between $BiMn_7O_{12}$ and $LaMn_7O_{12}$ could be the cause for the observed differences in physical properties,[6−9] in particular with respect to magnetism.

Acknowledgment. This work has received support from the Research Council of Norway, Grant 158518/431 (NANOMAT). We highly acknowledge the assistance from the research team at the Swiss−Norwegian Beamlines, ESRF.